Aeronautical Voice Radio Channel Modelling and Simulation – A Tutorial Review

Konrad Hofbauer[1,2] and Gernot Kubin[1]

[1] Graz University of Technology
SPSC – Signal Processing
and Speech Communication Laboratory
8010 Graz, Austria
konrad.hofbauer@tugraz.at
gernot.kubin@tugraz.at

[2] Eurocontrol Experimental Centre
INO – Innovative Research
91222 Brétigny-sur-Orge, France

***Abstract*— The basic concepts in the modelling and simulation of the mobile radio channel are reviewed. The time-variant channel is dominated by multipath propagation, Doppler effect, path loss and additive noise. Stochastic reference models in the equivalent complex baseband facilitate a compact mathematical description of the channel's input-output relationship. The realisation of these reference models as filtered Gaussian processes leads to practical implementations of frequency selective and frequency nonselective channel models.**

Three different small-scale area simulations of the aeronautical voice radio channel are presented. We demonstrate the practical implementation of a frequency flat fading channel. Based on a scenario in air/ground communication the parameters for the readily available simulators are derived. The resulting outputs give insight into the characteristics of the channel and serve as a basis for the design of digital transmission and measurement techniques.

I. Introduction

Air traffic control (ATC) has relied on the voice radio for communication between aircraft pilots and air traffic control operators since its beginning. The amplitude-modulation (AM) radio, which is in operation worldwide, has basically remained unchanged for decades. Given the aeronautical life cycle constraints, it is expected that the analogue radio will remain in use for ATC voice in Europe well beyond 2020 [1].

Eurocontrol Experimental Centre (France) and Graz University of Technology (Austria) are currently working on embedding supplementary digital data, such as the call-sign of the aircraft, into the voice signal of the analogue air/ground communication (see [2], [3], and Fig. 1). The radio transmission channel has a strong impact on the performance of such a speech watermarking system in terms of data rate and robustness. The degradation of the transmitted signal is studied for the purpose of system design and evaluation. This paper reviews the general concepts of radio channel modelling and demonstrates the use of simulators for the aeronautical voice channel.

Radio channel modelling has a long history and is a very active area of research. This is especially the case with respect to terrestrial mobile radio communications and wide-band data communications due to commercial interest.

However, the results are not always transferable to the aeronautical domain. A comprehensive up-to-date literature review on channel modelling and simulation with the aeronautical radio in mind is provided in [4]. It is highly recommended as a pointer for further reading and its content is not repeated here.

II. Basic Concepts

This and the following section are based on the work of Pätzold [5] and provide a summary of the basic characteristics, the modelling, and the simulation of the mobile radio channel. Another comprehensive treatment on this extensive topic is given in [6].

A. Amplitude Modulation and Complex Baseband

The aeronautical voice radio is based on the double-sideband amplitude modulation (DSB-AM, A3E or simply AM) of a sinusoidal, unsuppressed carrier [7]. An analogue baseband voice signal $x(t)$ which is band-limited to a bandwidth f_m modulates the amplitude of a sinusoidal carrier with amplitude A_0, carrier frequency f_c and initial phase φ_0. The modulated high frequency (HF) signal $x_{AM}(t)$ is defined as

$$x_{AM}(t) = (A_0 + kx(t))\cos(2\pi f_c t + \varphi_0)$$

with the modulation depth

$$m = \frac{|kx(t)|_{max}}{A_0} \leq 1$$

The real-valued HF signal can be equivalently written using complex notation and $\omega_c = 2\pi f_c$ as

$$x_{AM}(t) = Re\left\{(A_0 + kx(t))e^{j\omega_c t}e^{j\varphi_0}\right\} \quad (1)$$

Under the assumption that $f_c \gg f_m$ the HF signal can be demodulated and the input signal $x(t)$ reconstructed by detecting the envelope of the modulated sine wave. The absolute value is low-pass filtered and the original amplitude of the carrier is subtracted.

$$x(t) = \frac{1}{k}([|x_{AM}(t)|]_{LP} - A_0)$$

Fig. 2 shows the spectra of the baseband signal and the corresponding HF signal. Since the baseband signal is, by definition, low-pass filtered, the HF signal is a bandpass signal

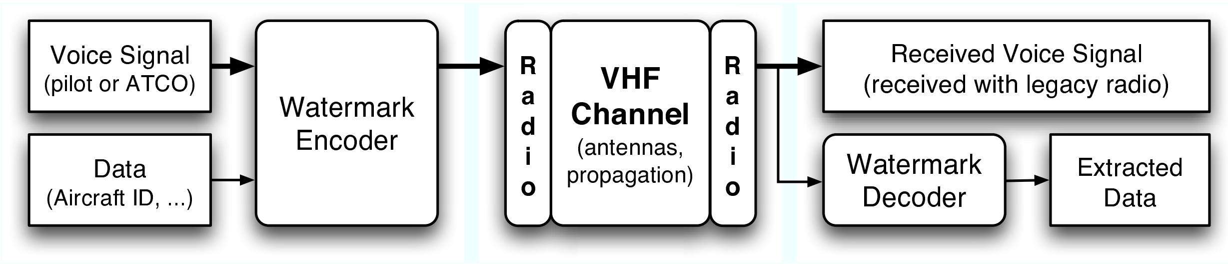

Fig. 1. General structure of a speech watermarking system for the aeronautical voice radio.

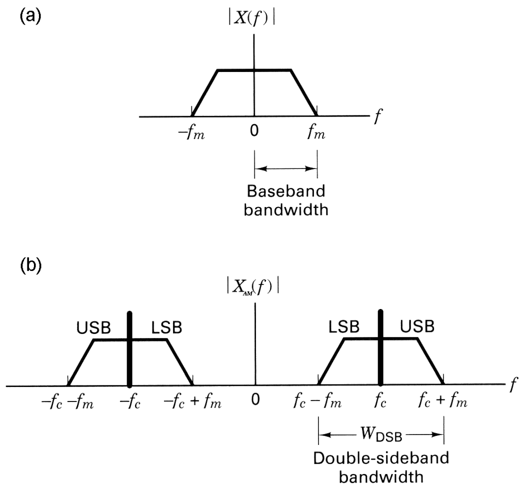

Fig. 2. Signal spectra of (a) the baseband signal $x(t)$ and (b) the HF signal $x_{AM}(t)$ with a carrier at f_c and symmetric upper and lower sidebands. [8, with modification]

and contains energy only around the carrier frequency and the lower and upper sidebands LSB and USB.

In general, any real bandpass signal $s(t)$ can be represented as the real part of a modulated complex signal,

$$s(t) = Re\left\{g(t)e^{j\omega_c t}\right\} \tag{2}$$

where $g(t)$ is called the *equivalent complex baseband* or *complex envelope* of $s(t)$ [8]. The complex envelope $g(t)$ is obtained by downconversion of the real passband signal $s(t)$, namely

$$g(t) = (s(t) + j\hat{s}(t))e^{-j\omega_C t}$$

with $\hat{s}(t)$ being the Hilbert transform of $s(t)$. The Hilbert transform removes the negative frequency component of $s(t)$ before downconversion [9]. A comparison of Eq. 1 and Eq. 2 reveals that the complex envelope $g_{AM}(t)$ of the amplitude modulated HF signal $x_{AM}(t)$ simplifies to

$$g_{AM}(t) = (A_0 + kx(t))e^{j\varphi_0}$$

The signal $x(t)$ is reconstructed from the equivalent complex baseband of the HF signal by demodulation with

$$x(t) = \frac{1}{k}\left(|g_{AM}(t)| - A_0\right) \tag{3}$$

The complex baseband signal can be pictured as a time-varying phasor or vector in a rotating complex plane. The rotating plane can be seen as a coordinate system for the vector, which rotates with the angular velocity ω_c.

In order to represent the HF signal as a *discrete-time* signal, it must be sampled with a frequency of more than twice the carrier frequency. This leads to a large number of samples and thus makes numerical simulation difficult even for very short signal durations. Together with the carrier frequency ω_c the complex envelope $g_{AM}(t)$ fully describes the HF signal $x_{AM}(t)$. The complex envelope $g_{AM}(t)$ has the same bandwidth $[-f_m; f_m]$ as the baseband signal $x(t)$. As a consequence it can be sampled with a much lower sampling frequency, which facilitates efficient numerical simulation without loss of generality. Most of the existing channel simulations are based on the complex baseband signal representation.

B. Mobile Radio Propagation Channel

Proakis [7] defines the communication channel as "… the physical medium that is used to send the signal from the transmitter to the receiver." Radio channel modelling usually also includes the transmitting and receiving antennas in the channel model.

1) Multipath Propagation: The transmitting medium in radio communications is the atmosphere or free space, into which the signal is coupled as electromagnetic energy by an antenna. The received electromagnetic signal can be a superposition of a line-of-sight path signal and multiple waves coming from different directions. This effect is known as *multipath propagation*. Depending on the geometric dimensions and the properties of the objects in a scene, an electromagnetic wave can be reflected, scattered, diffracted or absorbed on its way to the receiver.

From hereon we assume, without loss of generality, that the ground station transmits and the aircraft receives the radio signal. The effects treated in this paper are identical for both directions. As illustrated in Fig. 3, reflected waves have to travel a longer distance to the aircraft and therefore arrive with a time-delay compared to the line-of-sight signal. The received signal is spread in time and the channel is said to be *time dispersive*. The time delays correspond to phase shifts in between the superimposed waves and lead to constructive or destructive interference depending on the position of the aircraft. As both the position and the phase shifts change

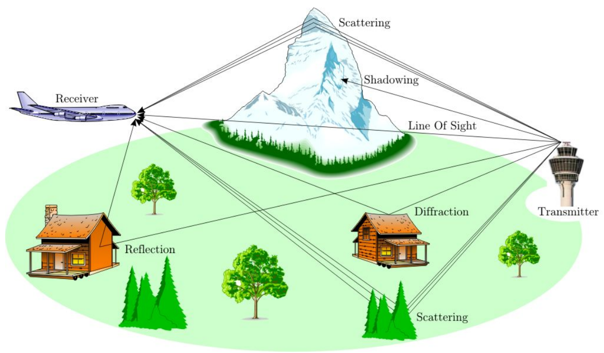

Fig. 3. Multipath propagation in an aeronautical radio scenario. [10]

constantly due to the movement of the aircraft, the signal undergoes strong pseudo-random amplitude fluctuations and the channel becomes a *fading channel*.

The *multipath spread* T_m is the time delay between the arrival of the line-of-sight component and the arrival of the latest scattered component. Its inverse $B_{CB} = \frac{1}{T_M}$ is the *coherence bandwidth* of the channel. If the *frequency bandwidth* W of the transmitted signal is larger than the coherence bandwidth ($W > B_{CB}$), the channel is said to be *frequency selective*. Otherwise, if $W < B_{CB}$, the channel is *frequency nonselective* or *flat fading*. This means that all the frequency components of the received signal are affected by the channel always in the same way [7].

2) Doppler Effect: The so-called *Doppler effect* shifts the frequency content of the received signal due to the movement of the aircraft relative to the transmitter. The Doppler frequency f_D, which is the difference between the transmitted and the received frequency, is dependent on the angle of arrival α of the electromagnetic wave relative to the heading of the aircraft.

$$f_D = f_{D,max}\cos(\alpha)$$

The maximum Doppler frequency $f_{D,max}$, which is the largest possible Doppler shift, is given by

$$f_{D,max} = \frac{v}{c} f_c \tag{4}$$

where v is the aircraft speed, f_c the carrier frequency and $c = 3 \cdot 10^8 \, \frac{\mathrm{m}}{\mathrm{s}}$ the speed of light.

The reflected waves arrive not only with different time-delays compared to the line-of-sight signal, but as well from different *directions* relative to the aircraft heading (Fig. 3). As a consequence, they undergo different Doppler shifts. This results in a continuous distribution of frequencies in the spectrum of the signal and leads to the so-called *Doppler power spectral density* or simply *Doppler spectrum*.

3) Channel Attenuation: The signal undergoes significant attenuation during transmission. The *path loss* is dependent on the distance d and the obstacles between transmitter and receiver. It is proportional to $\frac{1}{d^p}$, with the pathloss exponent p in the range of $2 \leq p < 4$. In the optimal case of line-of-sight free space propagation $p = 2$.

4) Additive Noise: During transmission *additive noise* is imposed onto the signal. The noise results, among others, from thermal noise in electronic components, from atmospheric noise or radio channel interference, or from man-made noise such as engine ignition noise.

5) Time Dependency: Most of the parameters described in this section vary over time due to the movement of the aircraft. As a consequence the response of the channel to a transmitted signal also varies, and the channel is said to be *time-variant*.

C. Stochastic Terms and Definitions

The following section recapitulates some basic stochastic terms in order to clarify the nomenclature and notation used here. The reader is encouraged to refer to [5] for exact definitions.

Let the *event* A be a collection of a number of possible *outcomes* s of a random experiment, with the real number $P(A)$ being its *probability* measure. A *random variable* μ is a mapping that assigns a real number $\mu(s)$ to every outcome s. The *cumulative distribution function*

$$F_\mu(x) = P(\mu \leq x) = P(\{s|\mu(s) \leq x\})$$

is the probability that the random variable μ is less or equal to x. The *probability density function* (*pdf*, or simply *density*) $p_\mu(x)$ is the derivative of the cumulative distribution function,

$$p_\mu(x) = \frac{dF_\mu(x)}{dx}$$

The most common probability density functions are the *uniform distribution*, where the density is constant over a certain interval and is zero outside, and the *Gaussian distribution* or *normal distribution* $N(m_\mu, \sigma_\mu^2)$, which is determined by the two parameters expected value m_μ and variance σ_μ^2.

With μ_1 and μ_2 being two statistically independent normally distributed random variables with identical variance σ_0^2, the new random variable $\zeta = \sqrt{\mu_1^2 + \mu_2^2}$ represents a *Rayleigh distributed* random variable (Fig. 4(a)). Given an additional real parameter ρ, the new random variable $\xi = \sqrt{(\mu_1 + \rho)^2 + \mu_2^2}$ is *Rice* or *Rician distributed* (Fig. 4(b)). A random variable $\lambda = e^\mu$ is said to be *lognormally distributed*. A multiplication of a Rayleigh and a lognormally distributed random variable $\eta = \zeta\lambda$ leads to the so-called *Suzuki distribution*.

A *stochastic process* $\mu(t, s)$ is a collection of random variables, which is indexed by a *time* index t. At a fixed time instant $t = t_0$, the value of a random process, $\mu(t_0, s)$, is a random variable. On the other hand, in the case of a fixed outcome $s = s_0$ of a random experiment, the value of the stochastic process $\mu(t, s_0)$ is a time function, or signal, that corresponds to the outcome s_0. As in common practise, the variable s is dropped in the notation for a stochastic process and $\mu(t)$ written instead. With $\mu_1(t)$ and $\mu_2(t)$ being two real-valued stochastic processes, a *complex-valued stochastic process* is defined by $\mu(t) = \mu_1(t) + j\mu_2(t)$. A stochastic process is called stationary if its statistical properties are invariant to a shift in time. The Fourier transform of the autocorrelation function of such a stationary process defines

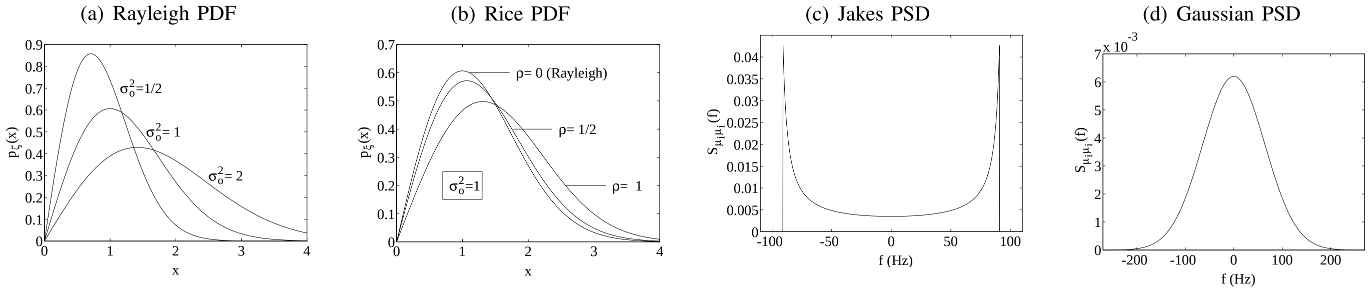

Fig. 4. Probability density functions (PDF) and power spectral densities (PSD, $f_{D,max} = 91\,\mathrm{Hz}$, $\sigma_0^2 = 1$) for Rayleigh and Rice channels. [5]

the *power spectral density* or *power density spectrum* of the stochastic process.

III. Radio Channel Modelling

Sec. II-B.1 illustrated the effect of multipath propagation from a geometrical point of view. However, geometrical *modelling* of the multipath propagation is possible only to a very limited extent. It requires detailed knowledge of the geometry of all objects in the scene and their electromagnetic properties. The resulting simulations are time consuming to set up and computationally expensive, and a number of simplifications have to be made. Furthermore the results are valid for the specific situation only and can not always be generalised. As a consequence, a stochastic description of the channel and its properties is widely used. It focuses on the distribution of parameters over time instead of trying to predict single values. This class of *stochastic channel models* is the subject of the following investigations.

In *large-scale* areas with dimensions larger than tens of wavelengths of the carrier frequency f_c, the local mean of the signal envelope fluctuates mainly due to shadowing and is found to be approximately lognormally distributed. This *slow-term fading* is important for channel availability, handover, and mobile radio network planning.

More important for the design of a digital transmission technique is the fast signal fluctuation, the *fast-term fading,* which occurs within small areas. As a consequence, we focus on models that are valid for *small-scale areas*, where we can assume the path loss and the local mean of the signal envelope due to shading, etc. , to be constant. Furthermore we assume for the moment a frequency nonselective channel and, for mathematical simplicity, the transmission of an unmodulated carrier.

A. Stochastic Mutlipath Reference Models

The sum $\mu(t)$ of all scattered components of the received signals can be assumed to be normally distributed. If we let $\mu_1(t)$ and $\mu_2(t)$ be two zero-mean statistically independent Gaussian processes with variance σ_0^2, then the sum of the scattered components is given in complex baseband representation as a zero-mean complex Gaussian process $\mu(t)$ and is defined by

$$\text{Scatter:} \qquad \mu(t) = \mu_1(t) + j\mu_2(t) \tag{5}$$

The line-of-sight (LOS) signal component $m(t)$ is given by

$$\text{LOS:} \qquad m(t) = A_0 e^{j(2\pi f_D + \varphi_0)} \tag{6}$$

again in complex baseband representation.

The superposition $\mu_m(t)$ of both signals is

$$\text{LOS+Scatter:} \qquad \mu_m(t) = m(t) + \mu(t) \tag{7}$$

Depending on the surroundings of the transmitter and the receiver, the received signal can consists of either the scatter components only or of a superposition of LOS and scatter components. In the first case (Eq. 5) the magnitude of the complex baseband signal $|\mu(t)|$ is Rayleigh distributed. Its phase $\angle(\mu(t))$ is uniformly distributed over the interval $[-\pi;\pi)$. This type of a *Rayleigh fading channel* is predominant in regions where the LOS component is blocked by obstacles, such as in urban areas with high buildings, etc.

In the second case where a LOS component and scatter components are present (Eq. 7), the magnitude of the complex baseband signal $|\mu(t) + m(t)|$ is Rice distributed. The Rice factor k is determined by the ratio of the power of the LOS component and the scatter components, where $k = \frac{A_0^2}{2\sigma_0^2}$. This *Rice fading channel* dominates the aeronautical radio channel.

One can derive the probability density of amplitude and phase of the received signal based on the Rice or Rayleigh distributions. As a further step, it is possible to compute the *level crossing rate* and the *average duration of fades*, which are important measures required for the optimisation of coding systems in order to address burst errors. The exact formulae can be found in [5] and are not reproduced here.

The power spectral density of the complex Gaussian random process in Eq. 7 corresponds to the Doppler power spectral density when considering the power of all components, their angle of arrival and the directivity of the receiving antenna. Assuming a Rayleigh channel with no LOS component, propagation in a two-dimensional plane and uniformly distributed angles of arrival, one obtains the so-called Jakes power spectral density as the resulting Doppler spectrum. Its shape is shown in Fig. 4(c).

However, both theoretical investigations and measurements have shown that the assumption that the angle of arrival of the scattered components is uniformly distributed does in practise not hold for aeronautical channels. This results in a Doppler spectrum which is significantly different from the

Jakes spectrum [11]. The Doppler power spectral density is therefore better approximated by a Gaussian power spectral density, which is plotted in Fig. 4(d). For nonuniformly distributed angles of arrival, as with explicit directional echos, the Gaussian Doppler PSD is unsymmetrical and shifted away from the origin. The characteristic parameters describing this are the *average Doppler shift* (the statistic mean) and the *Doppler spread* (the square root of the second central moment) of the Doppler PSD .

B. Realisation of the Reference Models

The above reference models are based on coloured Gaussian random processes. The *realisation* of these processes is not trivial and leads to the theory of deterministic processes. Mostly two fundamental methods are applied in the literature in order to generate coloured Gaussian processes. In the *filter method*, white Gaussian noise is filtered by an ideal linear time-invariant filter with the desired power spectrum. In the *Rice method* an infinite number of weighted sinusoids with equidistant frequencies and random phases are superimposed. In practise both methods can only approximate the coloured Gaussian process. Neither an *ideal* filter nor an *infinite* number of sinusoids can be realised. A large number of algorithms used to determine the actual parameters of the sinusoids in the Rice method exist. The methods approximate the Gaussian processes with a sum of a limited number of sinusoids, thus considering the computational expense [5]. For the filter method on the other hand, the problem boils down to filter design with its well-understood limitations.

C. Frequency Nonselective Channel Models

In frequency nonselective flat fading channels, all frequency components of the received signal are affected by the channel in the same way. *The channel is modelled by a multiplication of the transmitted signal with a suitable stochastic model process.* The Rice and Rayleigh processes described in Sec. III-A can serve as statistical model processes.

However it has been shown that the Rice and Rayleigh processes often do not provide enough flexibility to adapt to the statistics of real world channels. This has led to the development of more versatile stochastic model processes such as the Suzuki process and its variations (a product of a lognormal distribution for the slow fading and a Rayleigh distribution for the fast fading), the Loo Model with its variations, and the generalised Rice process.

D. Frequency Selective Channel Models

Where channel bandwidth and data rate increase, the propagation delays can no longer be ignored as compared to the symbol interval. The channel is then said to be frequency selective and over time the different frequency components of a signal are affected differently by the channel.

1) Tapped Delay Line Structure: For the modelling of a frequency selective channel, a tapped delay line structure is typically applied as reference model (Fig. 5). The ellipses model of Parsons and Bajwa [6] shows that all reflections and scatterings from objects located on an ellipse, with the transmitter and receiver in the focal points, undergo the same time delay. This leads to a complex Gaussian distribution of the received signal components for a given time delay, assuming a large number of objects with different reflection properties in the scene and applying the the central limit theorem. As a consequence, the tap weights $c_i(t)$ of the single paths are assumed to be uncorrelated complex Gaussian processes. It is shown in Sec. II-C that the amplitudes of the complex tap weights are then either Rayleigh or Rice distributed, depending on the mean of the Gaussian processes. An analytic expression for the phases of the tap weights can be found in [5].

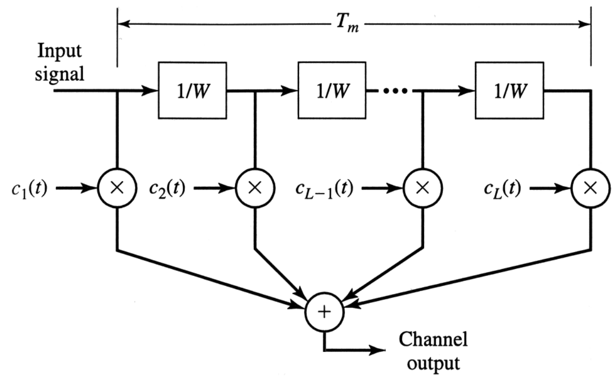

Fig. 5. Tapped delay line structure as a frequency selective and time variant channel model. W is the bandwidth of the transmitted signal, $c_i(t)$ are uncorrelated complex Gaussian processes. [5]

2) Linear Time-Variant System Description: The radio channel can be modelled as a linear time-variant system, with input and output signals in the complex baseband representation. The system can be fully subscribed by its time-variant impulse response $h(t, \tau)$. In order to establish a statistical description of the input/output relation of the above system, the channel is further considered as a stochastic system, with $h(t, \tau)$ as its stochastic system function.

These input/output relations of the stochastic channel can be significantly simplified assuming that the impulse response $h(t, \tau)$ is wide sense stationary[1] (*WSS*), and assuming that scattering components with different propagation delays are statistically uncorrelated (*U*ncorrelated *S*cattering).

Based on these two assumptions, Bello proposed in 1963 the class of *WSSUS* models. They are nowadays widely used and are of great importance in channel modelling. They are based on the tapped delay line structure and allow the computation of all correlation functions, power spectral densities and properties such as Doppler and delay spread, etc., from a given *scattering function*. The scattering function may be obtained by the measurement of real channels, by specification, or both. For example, the European working group 'COST 207' published scattering functions in terms of delay power spectral densities and Doppler power spectral densities for four

[1]Measurements have shown that this assumption is valid for areas smaller than tens of wavelengths of the carrier frequency f_c.

propagation environments which are claimed to be typical for mobile cellular communication.

E. AWGN Channel Model

The noise that is added to the transmitted signal during transmission is typically represented as an additive white Gaussian noise (AWGN) process. The main parameter of the model is the variance σ_0^2 of the Gaussian process, which together with the signal power defines the signal-to-noise ratio (SNR) of the output signal [7]. The AWGN channel is usually included as an additional block after the channel models described above.

IV. Voice Channel Simulation

This section aims to present three different simulators which implement the above radio channel models. We first define a simulation scenario based on which we show the simulators' input parameters and the resulting channel output. We use as example the aeronautical VHF voice radio channel between a fixed ground station and a general aviation aircraft which is flying at its maximum speed.

For all simulators the same pre- and post-processing of the input and output signals is used. It is based on a Matlab implementation of the filtering, amplitude modulation and demodulation in the equivalent complex baseband and receiver gain control. The input and output signals of all the simulators used are represented in the equivalent complex baseband.

A. Simulation Scenario and Parameters

For air-ground voice communication in civil air traffic control, the carrier frequency f_c is within a range from 118 MHz to 137 MHz, the 'very high frequency' (VHF) band. The 760 channels are spaced 25 kHz apart. The channel spacing is reduced to 8.33 kHz in specific regions of Europe in order to increase the number of available channels to a theoretical maximum of 2280. According to specification, the frequency response of the transmitter is required to be flat between 0.3 kHz to 2.5 kHz with a sharp cut-off below and above this frequency range [12].

For the simulation, we assume a carrier with amplitude $A_0 = 1$, frequency $f_c = 120\,\text{MHz}$ and initial phase $\varphi_0 = \frac{\pi}{4}$, a channel spacing of $W = 8.33\,\text{kHz}$, a modulation depth $m = 0.8$ and an input signal which is band-limited to $f_l = 300\,\text{Hz}$ to $f_m = 2.5\,\text{kHz}$. For the illustrations we use a purely sinusoidal baseband input signal $x(t) = \sin(2\pi f_a t)$ with $f_a = 500\,\text{Hz}$, which is sampled with a frequency of $f_{sa} = 8000\,\text{Hz}$ and bandpass filtered according to the above specification. Fig. 6 shows all values that the amplitude modulated signal $x_{AM}(t)$ takes during the observation interval in the equivalent complex baseband representation $g_{AM}(t)$. The white circle represents the *unmodulated* carrier signal, which is a single point in the equivalent complex baseband. A short segment of the magnitude of the signal, $|g_{AM}(t)|$, is also given.

In the propagation model a general aviation aircraft with a speed of $v = 60\,\frac{\text{m}}{\text{s}}$ is used. This results in a maximum Doppler frequency of $f_{D,max} = 24\,\text{Hz}$ (Eq. 4). Given the

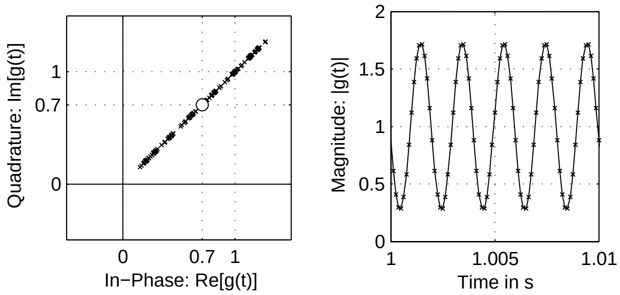

Fig. 6. Sinusoidal AM signal in equivalent complex baseband. Left: In-phase and quadrature components. The white circle indicates an unmodulated carrier. Right: The magnitude of $g(t)$.

carrier frequency f_c, the wavelength is $\lambda = \frac{c}{f_c} = 2.5\,\text{m}$. This distance λ is covered in $t_\lambda = 0.0417\,\text{s}$. Furthermore, we assume that the aircraft flies at a height of $h_2 = 3000\,\text{m}$ and at a distance of $d = 10\,\text{km}$ from the ground station. The ground antenna is taken to be mounted at a height of $h_1 = 20\,\text{m}$. The geometric path length difference Δl between the line-of-sight path and the dominant reflection along the vertical plane on the horizontal flat ground evaluates to

$$\Delta l = \sqrt{h_1^2 + \left(\frac{h_1 d}{h_1 + h_2}\right)^2} + \sqrt{h_2^2 + \left(d - \frac{h_1 d}{h_1 + h_2}\right)^2} - \sqrt{d^2 + (h_2 - h_1)^2} = 11.5\,\text{m}$$

which corresponds to a path delay of $\Delta\tau = 38.3\,\text{ns}$. In the worst case scenario of $T_m = 10\Delta\tau$, the coherence bandwidth is $B_{CB} = 2.6\,\text{MHz}$. With $B_{CB} \gg W$, according to Sec. II-B.1 the channel is surely frequency nonselective. Worst-case multipath spreads of $T_m = 200\,\mu\text{s}$ as reported in [11] cannot be explained with a reflection in the vertical plane, but only with a reflection on far-away steep slopes. In these rare cases, the resulting coherence bandwidth is in the same order of magnitude as the channel bandwidth.

We cannot confirm the rule of thumb given in [11] where $\Delta l \approx h_2$ given $d \gg h_2$. For example, a typical case for commercial aviation where $h_1 = 30\,\text{m}$, $h_2 = 8000\,\text{m}$ and $d = 100\,\text{km}$ results in a path difference of $\Delta l = 4.78\,\text{m}$. In the special case of a non-elevated ground antenna with $h_1 \approx 0$ the path delay vanishes. The Rician factor k is assumed to be $k = 12\,\text{dB}$, which corresponds to a fairly strong line-of-sight signal [11].

B. Mathworks Communications Toolbox Model

The Mathworks Communications Toolbox for Matlab [13] implements a multipath fading channel model. The simulator supports multiple fading paths, of which the first is Rice or Rayleigh distributed and the subsequent paths are Rayleigh distributed. The Doppler spectrum is approximated by the Jakes spectrum. As shown in Sec. III-A, the Jakes Doppler spectrum is not suitable for the aeronautical channel. The preferable Gaussian Doppler spectrum is unfortunately not supported by the simulator. The toolbox provides a convenient a tool for the visualisation of impulse and frequency response, gain and phasor of the multipath components, and the evolution of these quantities over time.

In terms of implementation, the toolbox models the channel as a time-variant linear FIR filter. Its tap-weights $g(m)$ are given by a sampled and truncated sum of shifted sinc functions. They are shifted by the path delays τ_k of the k^{th} path, weighted by the average power gain p_k of the corresponding path, and weighted by a random process $h_k(n)$. The uncorrelated random processes $h_k(n)$ are filtered Gaussian random processes with a Jakes power spectral density.

$$g(m) = \sum_k \operatorname{sinc}\left(\frac{\tau_k}{1/f_{sa}} - m\right) h_k(n) p_k$$

The equation shows once again that when all path delays are small as compared to the sample period, the sinc terms coincide. This result in a filter with only one tap and consequently in a frequency nonselective channel.

In our scenario the channel is frequency-flat, and a model according to Sec. III-C with one Rician path is appropriate. The only necessary input parameters for the channel model are f_{sa}, $f_{D,max}$ and k.

The output of the channel for the sinusoidal input signal as defined above is shown in Fig. 7(a). The demodulated signal (see Eq. 3 and Fig. 7(b)) reveals the amplitude fading of the channel due to the Rician distribution of the signal amplitude. It is worthwhile noticing that the distance between two maxima is roughly one wavelength λ. This fast-term fading results from the superposition of the line-of-sight component and the multitude of scattered components with Gaussian distribution. As mentioned above, this is under the small-scale area assumption where path loss and shading are assumed to be constant.

Fig. 7(c) and 7(d) show the demodulated signal after bandpass filtering and after automatic gain control, respectively. Amplitude modulations of the carrier wave with a frequency of less than $f_l = 0.3\,\text{kHz}$ are not caused by the input signal, as it is band-limited, but by the channel. These modulations scale the *entire* amplitude modulated carrier signal due to the frequency nonselectiveness of the channel. The automatic gain control can therefore detect these low-frequency modulations and compensate for them. This eliminates signal fading with frequencies of up to $f_l = 300\,\text{Hz}$.

The toolbox also allows a model structure with several discrete paths similar to Fig. 5. One can specify the delay and the average power of each path. A scenario similar to the first one with *two* distinct paths is shown for comparison. We define one Rician path with a Rician factor of $k = 200$. This means that it contains only the line of sight signal and no scattering. We furthermore define one Rayleigh path with a relative power of -12 dB and a time delay of $\Delta\tau = 38.3\,\text{ns}$, both relative to the LOS path.

Due to the small bandwidth of our channel, the results are equivalent to the first scenario. Fig. 8 shows the time-variation of the *power* of the two components, with the total power being normalised to 0 dB.

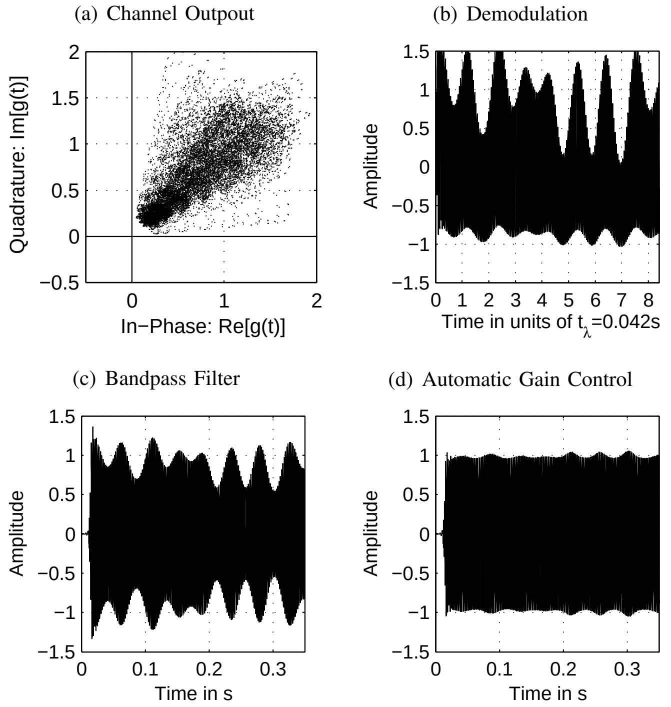

Fig. 7. Received signal at different processing stages. Received signal (channel output of Mathworks Communication Toolbox and an observation interval of 2 s) in equivalent complex baseband (a), after demodulation (b), after bandpass filtering (c), and after automatic gain control (d).

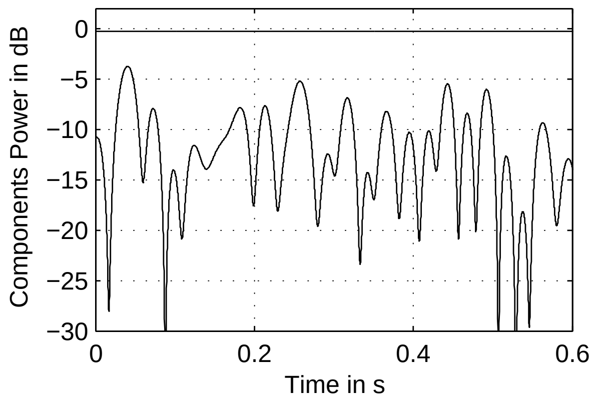

Fig. 8. Power of the line-of-sight component (top) and the Rayleigh distributed scattered components (bottom).

C. The Generic Channel Simulator

The Generic Channel Simulator (GCS) is a radio channel simulator which was developed between 1994 and 1998 under contract of the American Federal Aviation Administration (FAA). Its source code and documentation is provided in [14]. The GCS written in ANSI C and provides a graphical MOTIF-based interface and a command line interface to enter the model parameters. Data input and output files are in a binary floating point format and contain the signal in equivalent complex baseband representation. The last publicly available version of the software dates back to 1998. This version requires a fairly complex installation procedure and a number of adjustments in order to enable compiling of the source code on current operating systems. We provide some advice on how to install the software on the Mac OS X operating system and how to interface the simulator with Matlab [15].

The GCS allows the simulation of various types of mobile radio channels, the VHF air/ground channel among others. Similar to the Mathworks toolbox, the GCS simulates the radio channel by a time-variant IIR filter. The scatter path delay power spectrum shape is approximated by a decaying exponential multiplying a zeroth order modified Bessel function, the Doppler power spectrum is assumed to have a Gaussian shape.

In the following example we use a similar setup as in the second scenario in Sec. IV-B, a discrete line-of-sight signal and a randomly distributed scatter path with a power of -12 dB. With the same geometric configuration as above, the GCS software confirms our computed time delay of $\Delta\tau = 38.3$ ns.

Using the same parameters for speed, geometry, frequency, etc., as in the scenarios described above, we obtain a channel output as shown in Fig. 9.

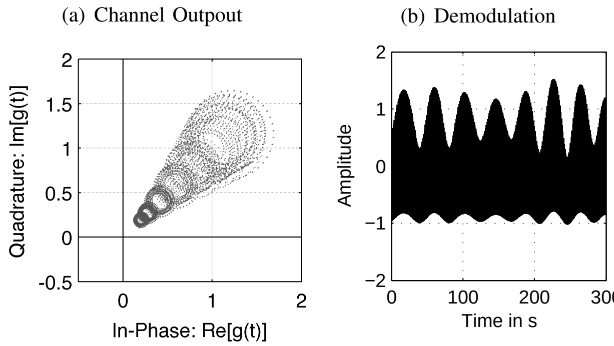

Fig. 9. Generic Channel Simulator: Received signal in an observation interval of 300 s (channel output) in equivalent complex baseband (a) and after demodulation (b).

The time axis in the plot of the demodulated signal is very different as compared to the one in Fig. 7(c). The amplitude fading of the signal has a similar shape as before but is in the order of *three magnitudes* slower than observed in Sec. IV-B. This contradicting result cannot be explained by the differing model assumptions, nor does it coincide with first informal channel measurements that we pursued.

We believe that the out-dated source code of the GCS has legacy issues which lead to problems with current operating system and compiler versions.

D. Direct Reference Model Implementation

The third channel simulation is based on a direct implementation of the concept described in Sec. III-C with the Matlab routines provided in [5]. We model the channel by multiplying the input signal with the complex random process $\mu_m(t)$ as given in Eq. 7. The random processes are generated with the sum of sinusoids approach as discussed in Sec. III-B. Fig. 10 shows the channel output using a Jakes Doppler PSD and a Rician reference model. The result is very similar to the one obtained with the Mathworks toolbox.

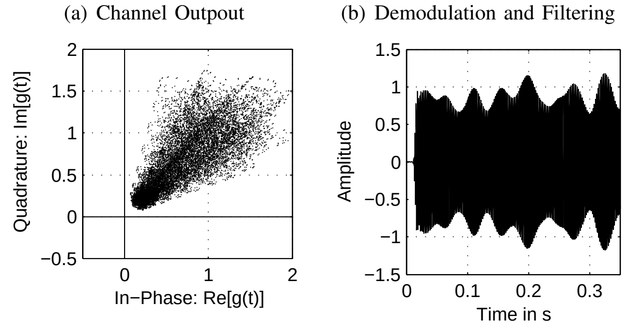

Fig. 10. Reference channel model with Jakes PSD: Received signal (channel output) in equivalent complex baseband (a) and after demodulation and bandpass filtering (b).

In a second example, a Gaussian distribution is used for the Doppler power spectral density instead of the Jakes model. The additional parameter $f_{D,co}$ describes the width of the Gaussian PSD by its 3 dB cut-off frequency. The value is arbitrarily set to $f_{D,co} = 0.3 f_{D,max}$. This corresponds to a fairly small Doppler spread of $B = 6.11$ Hz, compared to the Jakes PSD with $B = 17$ Hz. Fig. 11 shows the resulting discrete Gaussian PSD. The channel output in Fig. 12 confirms the smaller Doppler spread by a narrower lobe in the scatter plot. The amplitude fading is by a factor of two slower than with the Jakes PSD.

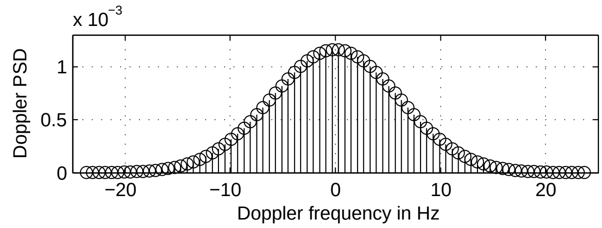

Fig. 11. Discrete Gaussian Doppler PSD with $f_{D,max} = 24$ Hz and a 3-dB-cut-off frequency of $f_{D,co} = 7.2$ Hz.

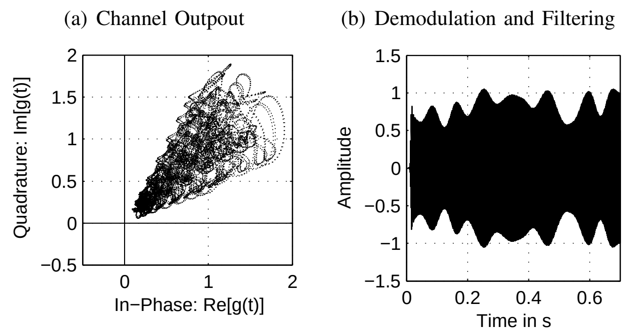

Fig. 12. Reference channel model with Gaussian PSD: Received signal (channel output) in equivalent complex baseband (a) and after demodulation and bandpass filtering (b).

V. Conclusion

The channel simulations presented here serve as a basis for the design of a measurement system to be used in upcoming tests on the aeronautical voice radio channel [16], [17]. The following example illustrates the usefulness of the simulations.

Fig. 13(a) shows the path gain of the frequency nonselective channel from the simulator in Sec. IV-B. Since the channel is flat fading, the path gain corresponds to the amplitude fading of the received signal. The magnitude spectrum of the path gain in Fig. 13(b) reveals that the maximum rate of change of the path gain approximately coincides with the maximum Doppler frequency $f_{D,max} = \frac{v}{c} f_c$ of the channel. The amplitude fading is band-limited to the maximum Doppler frequency.

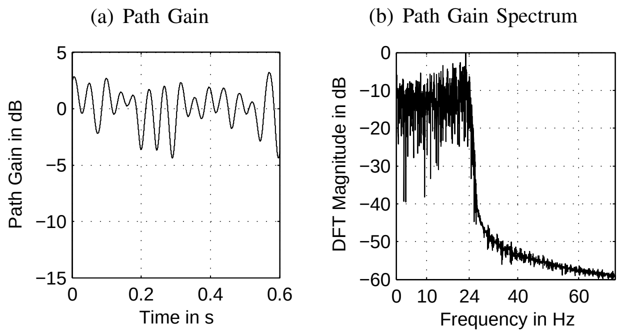

Fig. 13. Time-variant path gain and its magnitude spectrum for a flat fading channel with $f_{D,max} = 24$ Hz.

This fact can also be explained with the concept of *beat* as known in acoustics [18]. The superposition of two sinusoidal waves with slightly different frequencies f_1 and f_2 leads to a special type of interference, where the *envelope* of the resulting wave modulates with a frequency of $f_1 - f_2$.

The maximum frequency difference $f_1 - f_2$ between a scatter component and the carrier frequency f_c with which we demodulate in the simulation is given by the maximum Doppler frequency. This explains the band-limitation of the amplitude fading.

However, in a real world system a coherent receiver possibly demodulates the HF signal with a reconstructed carrier frequency $\hat{f}_c$ which is *already* Doppler shifted. In this case, the maximum frequency difference between Doppler shifted carrier and Doppler shifted scatter component is $2f_{D,max}$. This maximum occurs when the aircraft points towards the ground station so that the LOS signal arrives from in front of the aircraft, and when at the same time a scatter component arrives from the the back of the aircraft [11]. We can thereof conclude that the amplitude fading of the frequency nonselective aeronautical radio channel is band-limited to twice the maximum Doppler frequency $f_{D,max}$.

For a measurement system this now implies that the amplitude fading of the channel has to be sampled with at least double the frequency to avoid aliasing, so with a sampling frequency of $f_{ms} \geq 4f_{D,max}$. With the parameters used throughout this paper this means that the amplitude scaling has to sampled with a frequency of $f_{ms} = 96$ Hz or, in terms of a signal sampling rate $f_{sa} = 8000$ Hz, every 83 samples. For a measurement system based on maximum length sequences (MLS, see e.g. [8]) this means that the MLS length should be no longer than $L = 2^n - 1 = 63$ samples.

References

[1] D. van Roosbroek, "EATMP communications strategy," Eurocontrol, Technical Description Vol. 2 (Ed. 6.0), 2006.

[2] M. Hagmüller, H. Hering, A. Kröpfl, and G. Kubin, "Speech watermarking for air traffic control," in *Proceedings of the 12th European Signal Processing Conference (EUSIPCO'04)*, Vienna, Austria, September 2004.

[3] K. Hofbauer and H. Hering, "Digital signatures for the analogue radio," in *Proceedings of the 5th NASA Integrated Communications Navigation and Surveillance Conference (ICNS)*, Fairfax, USA, May 2005.

[4] BAE Systems Operations Ltd, "Literature review on terrestrial broadband VHF radio channel models," B-VHF, Report D-15, 2005. [Online]. Available: http:///www.B-VHF.org

[5] M. Pätzold, *Mobile Fading Channels. Modelling, Analysis and Simulation.* John Wiley and Sons Ltd., 2002.

[6] J. D. Parsons, *The Mobile Radio Propagation Channel.* John Wiley and Sons Ltd., 2000.

[7] J. G. Proakis and M. Salehi, *Communication Systems Engineering*, 2nd ed. Prentice Hall, 2001.

[8] B. Sklar, *Digital Communications*, 2nd ed. Prentice-Hall, 2001.

[9] J. R. Barry, E. A. Lee, and D. G. Messerschmitt, *Digital Communication*, 3rd ed. Springer-Verlag, 2004.

[10] E. Haas. Communications systems. [Online]. Available: http://www.kn-s.dlr.de/People/Haas/

[11] ——, "Aeronautical channel modeling," *IEEE Transactions on Vehicular Technology*, vol. 51, no. 2, 2002.

[12] ARINC, "Airborne VHF communications transceiver," Aeronautical Radio Inc., June 2003.

[13] The MathWorks, *MATLAB Communications Toolbox*, 3rd ed., 2004.

[14] K. Metzger. The generic channel simulator. [Online]. Available: http://www.eecs.umich.edu/genchansim/

[15] K. Hofbauer. The generic channel simulator. [Online]. Available: http://www.spsc.tugraz.at/people/hofbauer/gcs/

[16] K. Hofbauer, H. Hering, and G. Kubin, "Speech watermarking for the VHF radio channel," in *Proceedings of the 4th Eurocontrol Innovative Research Workshop*, Dec. 2005.

[17] ——, "A measurement system and measurements database for the aeronautical VHF voice channel," Feb. 2006, submitted for publication.

[18] M. Dickreiter, *Handbuch der Tonstudiotechnik.* KG Saur, 1997, vol. 1.